

Post processing of differential images for direct extrasolar planet detection from the ground

J.-F. Sauvage^a, L. Mugnier^a, T. Fusco^a and G. Rousset^{a, b}

^aONERA, BP-72, 92322 Châtillon Cedex, France;

^bLESIA, Observatoire de Paris, 5 place Jules Janssen, 92195 Meudon, France

ABSTRACT

The direct imaging from the ground of extrasolar planets has become today a major astronomical and biological focus. This kind of imaging requires simultaneously the use of a dedicated high performance Adaptive Optics [AO] system and a differential imaging camera in order to cancel out the flux coming from the star. In addition, the use of sophisticated post-processing techniques is mandatory to achieve the ultimate detection performance required. In the framework of the SPHERE project, we present here the development of a new technique, based on Maximum A Posteriori [MAP] approach, able to estimate parameters of a faint companion in the vicinity of a bright star, using the multi-wavelength images, the AO closed-loop data as well as some knowledge on non-common path and differential aberrations. Simulation results show a 10^{-5} detectivity at 5σ for angular separation around $15\frac{\lambda}{D}$ with only two images.

Keywords: Image processing, exoplanet detection, differential imaging, inverse problem, regularisation

1. INTRODUCTION

Today more than 150 exoplanets have been detected. But a great number among them are known by indirect gravitational effects on their parent star. This indirect detection and study allows one to estimate physical parameters of the companion, like its orbital period or mass, but does not indicate its atmosphere composition or its temperature. Exoplanet direct detection from the ground represents today a great scientific gain on our knowledge of exoplanet, since it allows one to perform spectroscopy of the planet. But such a detection needs a major improvement of technologies in use, since the star and its companion are separated by a fraction of arcsecond, and the flux ratio between them is extremely high (10^6). The SPHERE instrument,¹ a VLT Planet Finder, will allow to detect photons coming from hot Jupiter planets and will be installed on VLT in 2010. This instrument is composed of a high performance extreme AO system,² an optimised coronagraphic device³ and a dual band imager.⁴ But a dedicated post-processing method is mandatory in order to achieve the ultimate detection level of SPHERE. In this paper, we will consider the case of extreme AO coupled to differential imaging. The common use of spectral differential images is to perform differences between images at different wavelength in order to calibrate the residuals of aberration not corrected by AO and the residuals of diffraction not canceled by the coronagraph. The main limitation of differential imaging comes from differential aberrations between the two images, or between object images and reference images obtained at different times. The principle of differential imaging is detailed in the next section. We propose in the third section an optimised method dedicated to our specific issue, based on maximum a posteriori approach and able to estimate the turbulence parameters and the object in a pair of images. We present in the fourth section simulation results for the estimation of the turbulent phase structure function and the object.

2. SPECTRAL DIFFERENTIAL IMAGING

Spectral differential imaging is an instrumental method that aims at “attenuating” the flux of the central star with respect to the flux of the potential companion. This method was first initiated by Racine⁵ and Marois.⁴ Thus, differential imaging plays a role slightly similar to a coronagraph. The difference between differential imaging and a coronagraph is that a coronagraph subtracts only the coherent light to the signal, but before

email : jean-francois.sauvage@onera.fr

detection. Therefore photon noise in coronagraphic images is also attenuated. The differential imaging is able to subtract also the star light, but after detection. The photon noise variance in differential imaging is therefore doubled in the combined images. Spectral differential imaging consists in acquiring two simultaneous images of a system star-companion at different wavelengths. These two images are rescaled spatially and in intensity and combined in a subtraction that reduces the flux of central star and of the residual speckle. Here we will only treat differential imaging without coronagraph, for simplicity.

The subtraction should reduce the star light, but not the companion contribution in the image. This is possible if there are strong features in the companion spectrum. In the case of the giant gaseous exoplanets searched by the SPHERE project, a strong absorption band due to methane exists at $1.62\mu m$ and can be used in such a subtraction: the imaging wavelengths have to be chosen inside and outside the methane band (for example 1.575 and $1.625\mu m$), so that the companion emits at one wavelength, but is drastically less visible at the other one. On the other hand, the wavelengths have to be close enough to ensure the speckle pattern of the central star only differ in the two images by a spatial and intensity scaling.

Let us study the image formation theory and the limitation of differential imaging. The expression of the two images i_{λ_1} and i_{λ_2} can be written as a convolution of the observed object by the Point Spread Function [PSF] of the instrument plus additive noises due to photon statistics and electronics:

$$\begin{aligned} i_{\lambda_1}(\vec{\alpha}) &= h_{\lambda_1}(\vec{\alpha}) * o_{\lambda_1}(\vec{\alpha}) + n_1 \\ i_{\lambda_2}(\vec{\alpha}) &= h_{\lambda_2}(\vec{\alpha}) * o_{\lambda_2}(\vec{\alpha}) + n_2 \end{aligned} \quad (1)$$

with h_{λ_1} and h_{λ_2} the PSF's in the two imaging channels which depends on turbulence parameters and static aberrations in the imaging path, $\vec{\alpha}$ the angular position in the image field or the object field, o the observed object, $*$ stands for the convolution process, n_1 and n_2 stand for the noise in the images. For unresolved planets and star, the observed object is the sum of Dirac functions weighted by the total flux of the star and the companions at their respective position. The images are centred on the star, whose flux is supposed to be the same at the two wavelengths.

$$\begin{aligned} o_{\lambda_1}(\vec{\alpha}) &= F_0\delta(\vec{\alpha}_0) + \sum_i F_{1,i}\delta(\vec{\alpha}_i) \\ o_{\lambda_2}(\vec{\alpha}) &= F_0\delta(\vec{\alpha}_0) + \sum_i F_{2,i}\delta(\vec{\alpha}_i) \end{aligned} \quad (2)$$

with F_0 and $\vec{\alpha}_0$ the total flux and position of the central star, $F_{1,i}$, $F_{2,i}$ and $\vec{\alpha}_i$ the flux of the different companions at wavelengths λ_1 and λ_2 and their positions.

There are two different ways to perform image subtraction: the Single Difference [SD] cancels the effect of the common static aberrations, the Double Difference [DD] cancels the effect of both common and differential aberrations and is therefore photon noise limited.

- The SD consist in directly subtracting the two images and allows therefore to cancel the effect of the common aberrations in the two imaging channels. The images have to be spatially rescaled at the same wavelength by a $\frac{\lambda_2}{\lambda_1}$ dilation in the focal plane of the second image.

$$i_{SD}(\vec{\alpha}) \triangleq i_{\lambda_1}(\vec{\alpha}) - i_{\lambda_2}\left(\frac{\lambda_2}{\lambda_1}\vec{\alpha}\right) \quad (3)$$

If we consider the case where there is no differential aberration, and if λ_1 and λ_2 are sufficiently close then the PSF h_{λ_1} can be well approximated by h_{λ_2} rescaled at λ_1 . The limitation of this rescaling is $\frac{\Delta\lambda}{\lambda}$.⁴ Therefore the SD gives a good approximation of the difference of the companions convolved by first PSF h_{λ_1} , as the star light has been totally reduced:

$$i_{SD}(\vec{\alpha}) = \sum_i \left(F_{1,i} \delta(\vec{\alpha}_i) - \sum_i F_{2,i} \delta\left(\frac{\lambda_2}{\lambda_1} \vec{\alpha}_i\right) \right) * h_{\lambda_1} + n_1 - n_2 \quad (4)$$

But in a more realistic case, the static differential aberrations are not null and the difference between the image i_{λ_1} and the image i_{λ_2} rescaled at λ_1 makes appear the effect of differential aberrations.

The two images have to be acquired simultaneously in order to see the same acquisition conditions (turbulence parameters, guide star magnitude, AO performance...). Two imaging channels are therefore used, each of them acquiring an image centred on the imaging wavelength. The efficiency of this subtraction depends on differential aberration amplitude between the two optical imaging channels, since these aberrations are the main difference between the two combined images.⁶

- The DD aims at solving the SD limitation by using two reference images obtained on a reference star with the same imaging tool but at another time, the DD therefore cancels the effect of the differential aberrations (assuming that they have not evolved between the two observations):

$$i_{DD}(\vec{\alpha}) = \left(i_{\lambda_1}(\vec{\alpha}) - i_{\lambda_2}\left(\frac{\lambda_2}{\lambda_1} \vec{\alpha}\right) \right) - \left(i_{ref,\lambda_1}(\vec{\alpha}) - i_{ref,\lambda_2}\left(\frac{\lambda_2}{\lambda_1} \vec{\alpha}\right) \right) \quad (5)$$

The reference images are acquired at a different time, and on a different position on sky. This method is therefore sensitive to the evolution of the observing conditions between the acquisition of the two pairs of scientific and reference images. The evolution of turbulence parameters, AO performance, and most of all the evolution of quasi-static aberrations are the main limitations of the DD method.

3. POST PROCESSING FOR DIFFERENTIAL IMAGING

As explained before, the detection of low flux companions (contrast around 10^6 between central star and companion) requires the perfect calibration of both differential static aberrations and system parameters (AO performance). In a first approximation, we assume that the static aberrations in each imaging channel are perfectly known. This is well achieved by using a phase diversity calibration, as described by Sauvage et al.⁷ In this framework, we present here a new post-processing deconvolution method based on a MAP approach that estimates the turbulence-induced PSF and the observed object.

3.1. Separation static / turbulent aberrations in long exposure images

The image formation from the ground of stellar objects is perturbed by two factors: the atmospheric turbulence and the static aberrations of the telescope. The aberrant pupil phase is therefore the sum of two terms: $\phi = \phi_t + \phi_s$ with ϕ_t the turbulent part and ϕ_s the static part of the phase. The turbulent phase ϕ_t is a random variable of time and position in pupil plane and is therefore characterised by its structure function D_ϕ , whereas the static phase ϕ_s does not depend on time and is deterministically known. If the turbulent phase is stationary⁸ (as for uncorrected turbulence) then it has been shown by Roddier⁹ that the OTF is the product of the long exposure turbulence-induced OTF and of the static OTF:

$$\tilde{h}(\vec{f}) = \exp\left(-\frac{1}{2}D_\phi(\lambda\vec{f})\right) \frac{1}{S_{pup}} \iint_{S_{pup}} P(\vec{r} + \lambda\vec{f}) \exp\left(i\phi_s(\vec{r} + \lambda\vec{f})\right) \cdot P(\vec{r})^* \cdot \exp\left(-i\phi_s(\lambda\vec{f})\right) d^2\vec{r} \quad (6)$$

with

- $P(\vec{r})$ the pupil function
- $D_\phi(\lambda\vec{f})$ the atmospheric phase structure function after AO correction at wavelength λ :

$$D_{\phi_t}(\vec{\rho}) \triangleq \langle |\phi_t(\vec{r} + \vec{\rho}) - \phi_t(\vec{r})|^2 \rangle \quad (7)$$

The phase structure function $D_{\phi_t}(\lambda\vec{f})$ is a statistical term that quantifies the turbulent phase variations for two points separated by $\vec{\rho} = \lambda\vec{f}$ in the pupil plane and its shape depends on turbulence parameters and on AO performance. If the turbulence is corrected, D_ϕ depends both on \vec{r} and $\vec{\rho}$

$$D_{\phi_t}(\vec{r}, \vec{\rho}) = \langle |\phi_t(\vec{r} + \vec{\rho}) - \phi_t(\vec{r})|^2 \rangle \quad (8)$$

The average $\langle \cdot \rangle$ in the expression of $D_{\phi_t}(\vec{r}, \vec{\rho})$ is theoretically an average on phase occurrences (and thus on time), but may be approximated by an average $\langle \cdot \rangle_{\vec{r}}$ on \vec{r} (stationarity approximation). This simplified expression $D_{\phi_t}(\vec{\rho}) = \langle |\phi_t(\vec{r} + \vec{\rho}) - \phi_t(\vec{r})|^2 \rangle_{\vec{r}}$ is therefore independent of \vec{r} . This stationarity approximation is justifiable in the case of a Kolmogorov turbulence statistic, and often used also in the case of AO-corrected turbulent phases.⁸

Equation (6) shows that the global OTF is the product of a turbulence-induced OTF and a static OTF:

$$\tilde{h}(\vec{f}) = \tilde{h}_t(\vec{f}) \cdot \tilde{h}_s(\vec{f}) \quad (9)$$

with $\tilde{h}_t(\vec{f})$ the long exposure OTF due to turbulence only, and $\tilde{h}_s(\vec{f})$ the OTF due to telescope and the aberrations.

The structure function at a wavelength λ_2 can be rescaled at another wavelength λ_1 by the operation described in Equation 10, in order to compute the turbulence-induced OTF in the first image. Thus, the turbulent OTF \tilde{h}_{t,λ_1} in the first image can be computed thanks to this structure function at λ_2 by using relation 11. The image formation described in Equation 1 can now be rewritten as in Equation 12 taking explicitly into account the turbulent and static components of the phase.

$$D_{\phi_t,\lambda_1}(\vec{\rho}) = \left(\frac{\lambda_2}{\lambda_1}\right)^2 D_{\phi_t,\lambda_2}\left(\frac{\lambda_2}{\lambda_1}\vec{\rho}\right) \quad (10)$$

$$\tilde{h}_{t,\lambda_1} = \exp\left(-\frac{1}{2}\left(\frac{\lambda_2}{\lambda_1}\right)^2 D_{\phi_t,\lambda_2}\left(\frac{\lambda_2}{\lambda_1}\vec{\rho}\right)\right) \quad (11)$$

$$\begin{aligned} i_{\lambda_1}(\vec{\alpha}) &= h_{t,\lambda_1}(\vec{\alpha}) * h_{s,\lambda_1}(\vec{\alpha}) * o_{\lambda_1}(\vec{\alpha}) \\ i_{\lambda_2}(\vec{\alpha}) &= h_{t,\lambda_2}(\vec{\alpha}) * h_{s,\lambda_2}(\vec{\alpha}) * o_{\lambda_2}(\vec{\alpha}) \end{aligned} \quad (12)$$

with h_{t,λ_1} and h_{t,λ_2} the turbulent long exposure PSF depending on turbulent phase structure function $D_{\phi,\lambda}(\vec{\rho})$, h_{s,λ_1} and h_{s,λ_2} the PSF depending on static aberrations $\phi_{s,1}$ and $\phi_{s,2}$ in the two imaging channels.

3.2. The post-processing framework

The main limitation of differential imaging comes from differential aberrations in the two spectral channels which creates different static pattern in the images in the case of SD, and the evolution of these patterns due to system state modification in the case of DD. Therefore in our new approach we propose to estimate the PSF and the observed object o in the two images i_{λ_1} and i_{λ_2} . The estimation of the PSF reduces to that of its residual turbulent component as the static aberrations are supposed to be measured separately. The estimation is done thanks to the minimisation of an adequate MAP criterium $J(D_\phi, o)$.

The MAP approach is based on writing the probability $\mathcal{P} = P(o, D_\phi | i_{\lambda_1}, i_{\lambda_2})$ of a given object and D_ϕ knowing the images using Bayes' theorem (see Equation 13). Finding the best object and structure function means maximising the probability \mathcal{P} with respect to o and D_ϕ .

$$\mathcal{P}(o, D_\phi) = P(o, D_\phi | i_{\lambda_1}, i_{\lambda_2}) \propto P(i_{\lambda_1}, i_{\lambda_2} | o, D_\phi) \cdot P(o) \cdot P(D_\phi) \quad (13)$$

The first factor $P(i_{\lambda_1}, i_{\lambda_2} | o, D_\phi)$ is called ‘‘likelihood term’’ and embodies the relationship between data and the sought parameters. Its statistics is given by the noise statistics in the image (stationary white Gaussian

noise in a first approximation). The other probabilities are the *a priori* knowledge we have on the parameters to estimate. These regularisation terms allow to smooth the criterium and to accelerate its minimisation. For instance, the turbulent phase structure function has a particular shape depending on turbulence parameters and may therefore be taken into account in this regularisation term.

The criterium to minimise is $\mathcal{J} = -\ln(\mathcal{P})$ with \mathcal{P} written in Fourier space and may be rewritten as (Equation 14).

$$\begin{aligned} \mathcal{J}(D_\phi, o) &= \|\tilde{i}_{\lambda_1}(\vec{f}) - \tilde{h}_{t,\lambda_1}(D_\phi, \vec{f}) \cdot \tilde{h}_{s,\lambda_1}(\vec{f}) \cdot \tilde{o}_{\lambda_1}(\vec{f})\|^2 \\ &+ \|\tilde{i}_{\lambda_2}(\vec{f}) - \tilde{h}_{t,\lambda_2}(D_\phi, \vec{f}) \cdot \tilde{h}_{s,\lambda_2}(\vec{f}) \cdot \tilde{o}_{\lambda_2}(\vec{f})\|^2 \\ &+ \mathcal{J}_{R,D_\phi}(D_\phi) + \mathcal{J}_{R,o}(o) \end{aligned} \quad (14)$$

where $\tilde{\cdot}$ denotes the Fourier transform, \mathcal{J}_{R,D_ϕ} and $\mathcal{J}_{R,o}$ denote regularisation terms accounting for *a priori* knowledge we may have on the parameters to estimate.

3.3. Assumption and subsequent simplified method

In the framework of this deconvolution process, we make the following assumption in order to simplify the minimisation and demonstrate the feasibility of such a global technique:

We assume that the companion presents particular spectral signature : it emits light at the first wavelength and is totally undetectable at the second wavelength, it means the object is an ideal hot Jupiter and presents strong absorption line around $1.6\mu\text{m}$. The second image i_{λ_2} can therefore be seen as a calibration PSF, and the global minimisation may be approximated by the three following steps :

- 1) Estimation of the structure function $D_\phi(\lambda_2 \cdot \vec{f})$ in the image i_{λ_2} without the object, knowing the static aberration. This corresponds to the minimisation of the two middle term with respect to D_ϕ in Equation 14: likelihood term on i_{λ_2} , and regularisation term on D_ϕ .
- 2) Rescaling of the structure function (estimated at λ_2) at wavelength λ_1 according to Equation 10 and computation of global PSF h_1 of the first image i_{λ_1} , knowing the static aberration of the first channel according to Equation 11.
- 3) Deconvolution of the first image with the previously computed PSF h_1 , and estimation of the object in i_{λ_1} . This corresponds to the minimisation of the two terms depending on o only (first and last) in the criterium \mathcal{J} with respect to o .

3.4. Estimation of phase structure function D_ϕ

The turbulent phase structure function gives a statistical knowledge on a turbulent phase. For a turbulent phase following a Kolmogorov profile, the structure function is given by the relation $D_\phi(\rho) = (\frac{\rho}{r_0})^{\frac{5}{3}}$, with r_0 the Fried parameter. But for a turbulent phase corrected by an AO system, this relation takes into account the AO system parameters and is here numerically estimated. The Figure 1 shows typical profiles of D_ϕ for the turbulence and AO conditions explained in section 4, with variations of seeing.

Let us study the first step of the method : the estimation of structure function D_ϕ in a calibration long exposure PSF. A criterium (see Equation 15) is used for this minimisation, based on the likelihood term and a regularisation term on D_ϕ .

$$\begin{aligned} \mathcal{J}(D_\phi) &= \|\tilde{i}_{\lambda_2} - F \cdot \exp(-\frac{1}{2}D_\phi) \cdot \tilde{h}_{s,\lambda_2}\|^2 \\ &+ \mathcal{J}_{D_\phi}(D_\phi) \end{aligned} \quad (15)$$

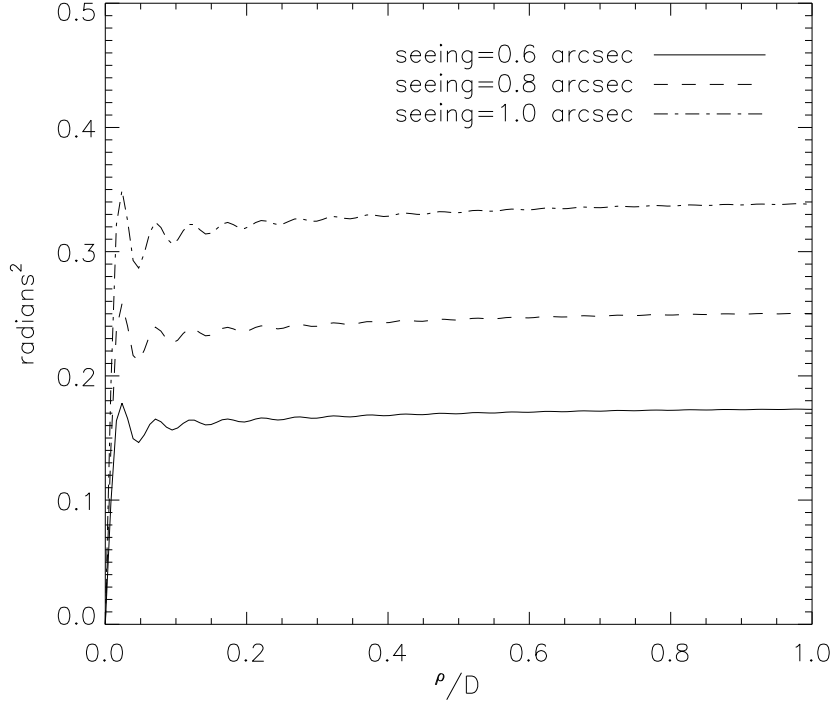


Figure 1. Profiles of phase structure function for a turbulent phase corrected by AO. Condition of simulation : Paranal + SAXO, with different values of seeing.

with F the flux of the observed star, D_ϕ the structure function to estimate and \tilde{h}_{s,λ_2} the static PSF due to static aberration. D_ϕ is the only estimated parameter, since the star flux as well as the static aberrations (and therefore the static PSF) are assumed to be known.

The regularisation term $\mathcal{J}_{D_\phi}(D_\phi)$ is an adaptive smoothness term on estimated D_ϕ designed to avoid noise amplification during estimation and to allow the extrapolation of D_ϕ to regions where the static OTF is very small (or even null). The regularisation is done using the gradient of structure function ∇D_ϕ and penalises deviations between two adjacent pixels according to a typical adaptive variance, depending on pixel position. This term is computed as explained in Equation 16.

$$\mathcal{J}_{D_\phi}(D_\phi) = \frac{1}{2} (\nabla D_\phi)^t C_{\nabla D_\phi}^{-1} (\nabla D_\phi) \quad (16)$$

with $C_{\nabla D_\phi}$ the covariance matrix of the gradient of phase structure function ∇D_ϕ . This covariance matrix has been estimated on different occurrences of ∇D_ϕ , these occurrences have been generated with different value for r_0 , wind speed or star magnitude. $C_{\nabla D_\phi}$ quantifies the typical variability of ∇D_ϕ and allows one to correctly weigh the regularisation term. A common issue in regularised inversion methods and criterium minimisation is how to choose the hyperparameter, that balances the two terms of the criterium. With the Bayesian approach adapted here and with the use of a $C_{\nabla D_\phi}$ estimated by simulations, there is no such hyper-parameter to be tuned and the estimation of D_ϕ is completely unsupervised.

3.5. Object estimation

In our procedure, the structure function and the object estimation are done sequentially. This simplified approach gives a good idea of the global approach performance, even though a global minimisation should be even more precise and therefore lead to a slightly better object estimation (which is the final goal).

The object estimation is done using MISTRAL¹⁰ algorithm developed at ONERA. This algorithm is based on the minimisation of the following criterium, and gives the best object given an image, its PSF and *a priori* knowledge:

$$\mathcal{J}(o) = \|i_{\lambda_1} - \hat{h}_{t,\lambda_1} * h_{s,\lambda_1} * o\|^2 + \mathcal{J}_R(o) \quad (17)$$

with \hat{h}_{t,λ_1} the turbulent PSF at λ_1 computed with the estimated D_ϕ , $\mathcal{J}_R(o)$ a regularisation term accounting for *a priori* knowledge on the object. This regularisation term may contains different terms. In our particular problematic, we used a positivity constraint and a quadratic linear-quadratic regularisation.¹⁰

4. RESULTS

In this section, we validate our post-processing method on simulated data. The simulation conditions are detailed in the following list, and correspond to a 8m class Telescope with an Adaptive Optics system of high performance like SPHERE, and a turbulence profile corresponding to a typical Paranal sky. The goal of this simulation is to compare the detectivity of Single Difference, Double Difference and our approach.

Conditions :

- $\lambda_1 = 1.60\mu m$, $\lambda_2 = 1.58\mu m$ (corresponding to two wavelengths inside and outside the methane absorption line)
- Turbulence parameter : a typical Cn^2 profile for Paranal is being used with an average wind speed of 12.5 m/s, and seeing of 0.8 arcseconds.
- Adaptive Optics parameters : as extreme-AO. 41×41 actuators with spatially filtered Shack Hartmann WFS, a L3CCD working at 1.2kHz sampling frequency. The guide star has a V-magnitude of 8.
- The static aberration component is randomly generated according to a $\frac{1}{n^2}$ spectrum (n being the radial Zernike order) with 1300 Zernike coefficients and a differential wavefront error of 10nm RMS in each channel. i.e., the total differential wavefront error is 14nm RMS.
- Imaging parameters : 256×256 images, with a 8m telescope. The different PSF's h_{λ_i} are generated at Shannon (i.e., one pixel is $\frac{\lambda_i}{2D}$ arcsecond on sky) and are therefore already spatially rescaled. The images i_{λ_1} and i_{λ_2} are generated by convolution of the object and the PSF of each channel.
- The object at the first wavelength is a star and three companions with a flux ratio of 10^{-3} for the first image, and the star alone for the object at the second wavelength. The star flux is set to a total of 10^7 photons for each wavelength. The companions are located close to the star, respectively at 2.5, 5.0 and 7.5 $\frac{\lambda}{D}$.

Such conditions allow us to generate quite realistic images (see example on Figure 2) that are processed by our method.

4.1. D_ϕ estimation : simulation results

The image i_{λ_2} is processed in order to estimate the phase structure function via the minimisation of the criterium presented in previous section. Figure 3 shows results of D_ϕ estimation. The true D_ϕ (used to generate the images) on the left shows the plateau value and central features characteristic of AO system. In the middle, the estimated structure function without regularisation (only the likelihood term is used in the criterium). Noise on the edge of the circular support of D_ϕ is amplified. The use of adaptive regularisation (on the right) allows us to reduce this noise amplification and gives a far better estimation of D_ϕ . The error profiles are plotted on Figure 4.

Without regularisation, the error is lower than 0.03 rad². Figure 4 shows the gain brought by regularisation on D_ϕ estimation : the maximum error for high frequencies is one order of magnitude fainter when regularisation is used during D_ϕ estimation.

The adaptive aspect of the regularisation allows a powerful smoothing of the estimated D_ϕ at the edges, and simultaneously a data-driven precise estimation of the quite oscillating D_ϕ near the center.

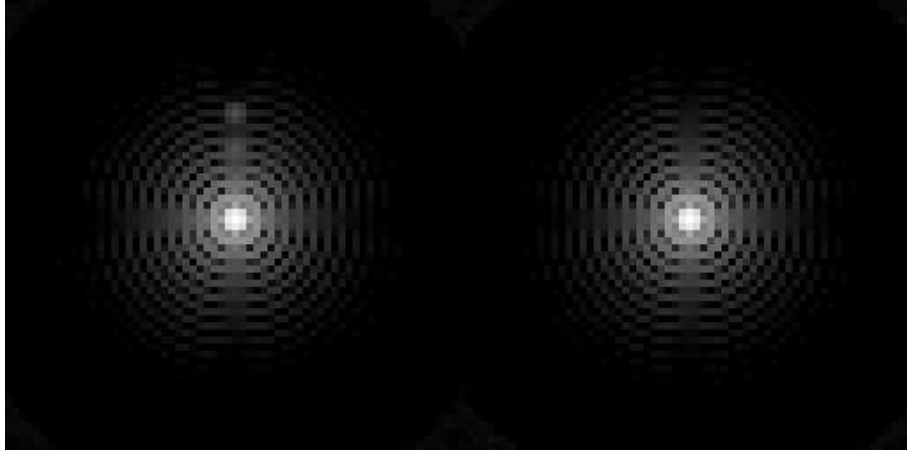


Figure 2. Example of spectral images, logarithmic scale, two of the three companions around the central star are visible on the left image ($\lambda_1 = 1.6\mu m$), and only the star in the right image ($\lambda_2 = 1.58\mu m$).

4.2. Computation of h_1

The D_ϕ estimated at λ_2 is now used to compute h_1 , the PSF of the first image. This computed PSF will then be used in the deconvolution of the first image i_{λ_1} . Once again we assume to know perfectly the static aberrations of first imaging channel. The OTF \tilde{h}_1 is thus computed as product of turbulent OTF and static OTF by mean of Equations (9), (10) and (11).

4.3. Object estimation

One can estimate different objects with the different D_ϕ estimated previously : the rough D_ϕ without regularisation, regularised D_ϕ or by using the true D_ϕ , used for images simulation. The different objects estimated are gathered in Figure 5, and compared with results of differential imaging in different cases.

[Top left] The observed object. Central star has a total flux of 10^7 photon, the three companions have a ratio of 10^{-3} compared to central star and are situated at 2.5 , 5.0 and $7.5 \frac{\lambda}{D}$ inside the AO halo.

[Top middle] result of single differential imaging. The two images at λ_1 and λ_2 are spatially rescaled before subtraction. The effect of differential aberrations on central star reduces contrast around it, the first companion is unseeable and the second one is visible.

[Top right] result of double differential imaging. A difference of reference images has been subtracted to the single difference of images. This combination of images plays the role of a calibration of differential aberrations and allows to reduce their effect. This result is ideal since it does not account for slow variations of static aberrations between the two images, of evolution of turbulence parameters between the acquisition of object images and reference images. It is therefore a perfect DD, only limited by photon noise.

[Bottom left] object estimated after deconvolution by the PSF h_{1,D_ϕ} . This PSF has been computed with estimated D_ϕ with regularisation. The two farrest companions are clearly visible, the flux ratio is almost respected. The closest companion is quite visible, but a bit hidden by residual flux coming from the central star.

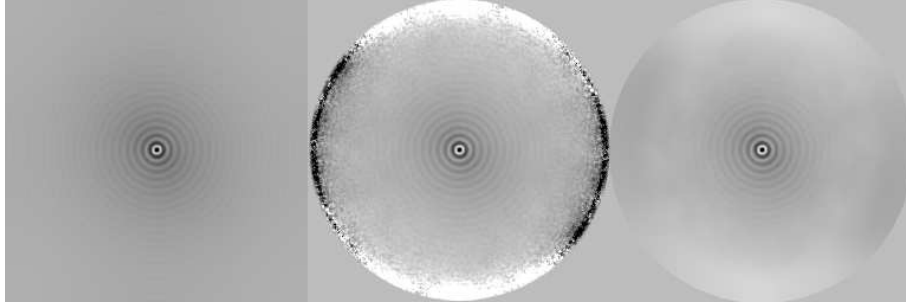


Figure 3. True D_ϕ , D_ϕ estimated without regularisation, D_ϕ estimated with regularisation.

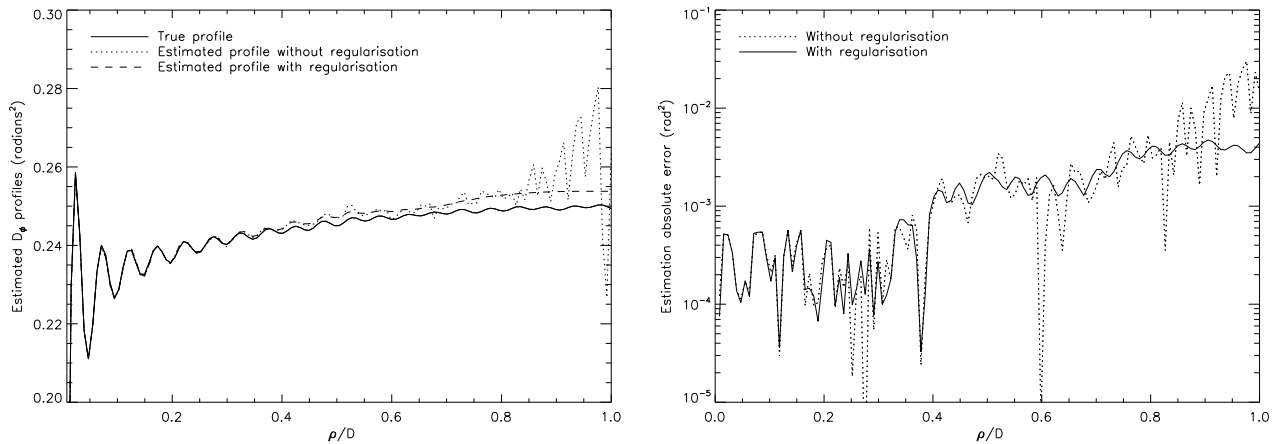


Figure 4. X cross-section for [left] true and estimated structure function with and without regularisation, and [right] absolute error on estimated structure function with and without regularisation.

[Bottom right] object estimated after deconvolution with the PSF obtained with regularised D_ϕ . The noise in this object is slightly fainter than in the previous one, and the central star and the first object are better defined.

5. PERFORMANCE EVALUATION

The method performance is evaluated here by the 5σ detectivity profiles. Detectivity profile is obtained as 5 times the standard deviation computed azimuthally on the result of Single Difference, Double Difference, and object estimation by our approach normalised to peak flux in image.

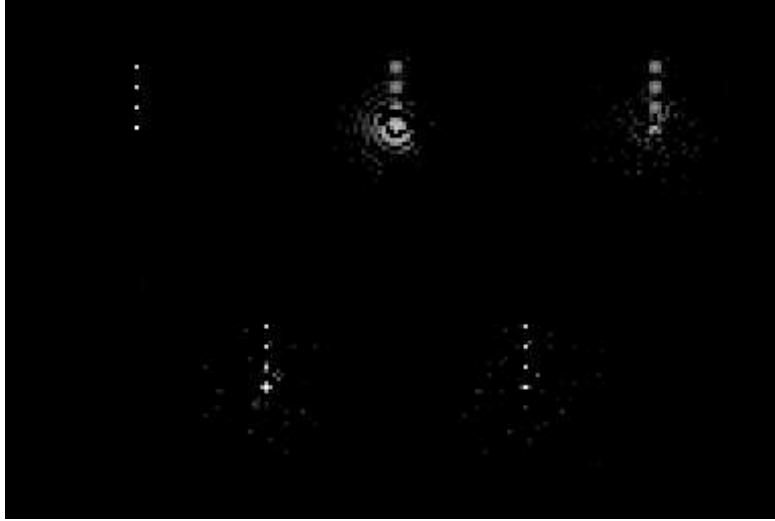


Figure 5. logarithmic scale of [Top left] observed object, and result of [Top middle] SD and [Top right] DD, [Bottom left] deconvolved object with the PSF computed with non-regularised structure functions, [Bottom right] deconvolved object with the PSF computed with regularised structure function.

These detectivity profiles are shown on Figure 6. The simulation conditions are the one listed on section 4. As the static differential aberrations are weak (10nm RMS on each imaging channel), the DD is better than SD only close to optical axis (closer than $5\frac{\lambda}{D}$) when differential aberrations effects dominates. Far from the optical axis, the two differences are photon noise limited and the SD gives therefore slightly better detectivity. We found the expected gain in $\sqrt{2}$. Whatever the angular separation, our method gives better detectivity. The gain is more than 5 in the whole field of view. It is due both to the concentration of the object light in one pixel and to photon noise reduction due to our regularised deconvolution.

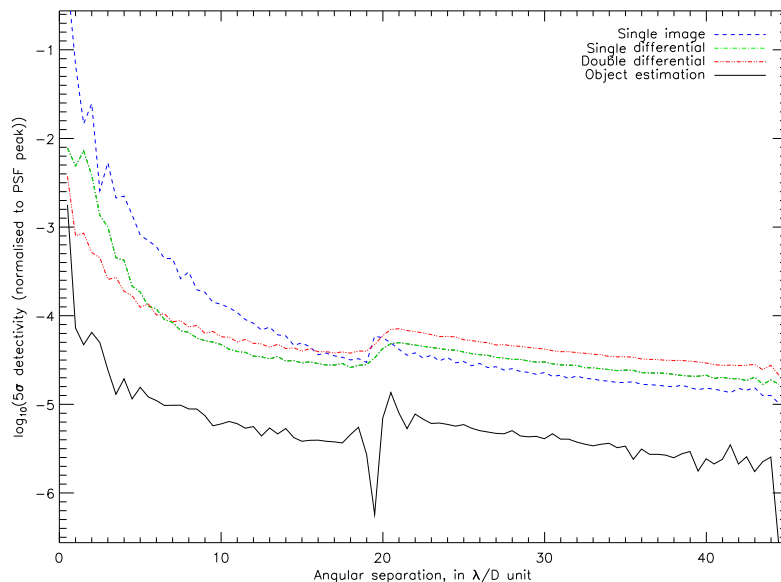


Figure 6. Averaged detection profiles at 5σ in the case of rough image, Single difference, double difference and our simplified object estimation.

6. CONCLUSION

We propose a method which allows to solve SD limitations (differential aberrations) and gives better results than DD, without reference images. In a perfect case, detectivity at 5σ reaches less than 10^{-5} at $15\frac{\lambda}{D}$. This result has still to be tested in more complex cases (slowly evolving static aberrations or mis-calibration, residual background) but gives a rough idea of the potentiality of the method. The perspectives for this method are to perform a global estimation of the parameters (structure function, object in the two images and static aberrations), to process real images obtained on a differential imager like NACO SDI, and to generalise our approach to coronagraphy.

REFERENCES

1. J.-L. Beuzit, D. Mouillet, C. Moutou, K. Dohlen, P. Puget, T. Fusco, and A. e. a. Boccaletti, “A planet finder instrument for the vlt,” in *IAUC 200, Direct Imaging of Exoplanets: Science & Techniques*, 2005. Conference date: Oct. 2005, Nice, France.
2. T. Fusco, G. Rousset, J.-L. Beuzit, D. Mouillet, K. Dohlen, R. Conan, C. Petit, and G. Montagnier, “Conceptual design of an extreme ao dedicated to extra-solar planet detection by the vlt-planet finder instrument,” in *Astronomical Adaptive Optics Systems and Applications II*, **5903**, Proc. Soc. Photo-Opt. Instrum. Eng., SPIE, 2005. Conference date: July2005, San Diego, USA.
3. A. Boccaletti, P. Riaud, P. Baudoz, J. Baudrand, D. Rouan, D. Gratadour, F. Lacombe, and A.-M. Lagrange, “The four-quadrant phase-mask coronagraph. IV. first light at the very large telescope,” *Pub. Astron. Soc. Pacific* **112**, p. 1479, 2004.
4. C. Marois, *Direct Exoplanet Imaging around Sun-like Stars: Beating the Speckle Noise with Innovative Imaging Techniques*. PhD thesis, Université de Montréal, 2004.
5. R. Racine, G. A. Walker, D. Nadeau, and C. Marois, “Speckle noise and the detection of faint companions,” *Pub. Astron. Soc. Pacific* **112**, p. 587, 1999.
6. A. Boccaletti, D. Mouillet, T. Fusco, P. Baudoz, C. Cavarroc, J.-L. Beuzit, C. Moutou, and K. Dohlen, “Analysis of ground-based differential imager performance,” in *IAUC 200, Direct Imaging of Exoplanets: Science & Techniques*, 2005. Conference date: Oct. 2005, Nice, France.

7. J.-F. Sauvage, T. Fusco, G. Rousset, C. Petit, A. Blanc, and J.-L. Beuzit, "Fine calibration and pre-compensation of ncpa for high performance ao system," in *Advancements in Adaptive Optics*, **5903**, pspie, SPIE, 2005. Conference date: June 2005, San Diego, USA.
8. J.-M. Conan, *Étude de la correction partielle en optique adaptative*. PhD thesis, Université Paris XI Orsay, Oct. 1994.
9. F. Roddier, "The effects of atmospherical turbulence in optical astronomy," in *Progress in Optics*, E. Wolf, ed., **XIX**, pp. 281–376, North Holland, Amsterdam, 1981.
10. L. M. Mugnier, T. Fusco, and J.-M. Conan, "MISTRAL: a myopic edge-preserving image restoration method, with application to astronomical adaptive-optics-corrected long-exposure images.," *J. Opt. Soc. Am. A* **21**, pp. 1841–1854, Oct. 2004.